JOURNAL OF MATERIALS SCIENCE: MATERIALS IN MEDICINE 14 (2003) 985–990

Crystallization modifies osteoconductivity in an apatite–mullite glass–ceramic

C. O. FREEMAN*, I. M. BROOK, A. JOHNSON, P. V. HATTON
Centre for Biomaterials and Tissue Engineering, University of Sheffield, School of Clinical Dentistry, Claremont Crescent, Sheffield, S10 2TA, UK
E-mail: c.o.freeman@sheffield.ac.uk

R. G. HILL
Department of Materials Science, Imperial College of Science and Technology, London, UK

K. T. STANTON
Department of Materials Science and Technology, University of Limerick, Limerick, Ireland

The response to implantation of novel apatite glass–ceramics was evaluated using a weight bearing *in vivo* bone implant model. Five novel glasses with varying calcium to phosphate ratios were cast as short rods and heat-treated to crystallize principally apatite. One glass ceramic had an apatite stoichiometry (Ca : P = 1.67); three were phosphate-rich and one calcium-rich. One of the phosphate-rich glasses was also tested in its glassy state to determine the effect of crystallization on the biological response. Rods were implanted into the midshaft of rat femurs and left for 28 days. The femurs were then harvested and processed for scanning electron microscopy, energy dispersive X-ray microanalysis and conventional histology as ground and polished sections. Four of the materials exhibited evidence of osseointegration and osteoconduction. However, there was a marked inflammatory response to one of the phosphate-rich glass–ceramics, and to the non-crystallized glass. Crystallization of the latter significantly improved the bone tissue response. The glass–ceramic with an apatite stoichiometry elicited the most favorable response and merited further study as an osteoconductive bone substitute in maxillofacial and orthopedic surgery.

1. Introduction

Bone defects resulting from trauma, disease or developmental anomalies often require surgical repair and reconstruction. Local reconstruction via osteotomy or distraction can be complex and may lead to significant local morbidity; furthermore, these techniques may not address the need for bone augmentation. Autogenous bone grafting increases morbidity because of the need for an additional surgical procedure with an increase in surgical time and complexity. There is a limit to the amount and quality of bone available at donor sites and it may prove difficult to produce grafts of the required shape. Alternative augmentation techniques using products derived from animals can meet with resistance because of the potential for disease transmission; there may also be objections on the basis of ecological, cultural and religious considerations. Despite the development of a wide range of materials for use in reconstructive surgery there remain difficulties with long-term integration, migration of particulate materials, exfoliation of grafts and poor biomechanical properties; these factors reduce usefulness and hinder clinical acceptability. There is a clinical need to develop new materials that are osteoconductive and with good mechanical properties, which could be economically produced, in a variety of shapes (including custom shapes) to repair bone defects and augment bone volume.

Glasses are often castable at low processing temperatures ($< 1300\,^{\circ}\mathrm{C}$) and, with the correct compositions and heat treatment, can be crystallized to obtain glass–ceramics with only low levels of residual glass. These materials may achieve bend strength and fracture toughness in excess of 250 MPa and $2.5\,\mathrm{MPa}\sqrt{\mathrm{m}}$, respectively. These mechanical properties are very significant for weight-bearing applications [1]. Ionomer glasses and ionomeric (glass polyalkenoate) cements have been shown to exhibit osteoconduction [2] and have been clinically successful for orthopedic weight-bearing applications [3]. Ionomer glasses can be cast to shape using the lost wax technique with standard dental laboratory equipment which is conventionally used to cast precious metal alloys and thus there is potential for production of custom made implants [4]. It has been demonstrated that ionomer glasses can bulk nucleate to

*Author to whom all correspondence should be addressed.

TABLE I Heat treatment and nucleation hold temperatures used to crystallize glasses to apatite

	LG112	LG113	LG114	LG185	LG3
Nucleation °C (1 h)	660	675	680	670	743
Ceramming °C (1 h)	893/1040*	834	771	893	976

*Mullite phase.

give principally fluorapatite ($Ca_5(PO_4)_3F$, which is analogous to the hydroxyapatite phase of tooth and bone. The fluorapatite forms as elongated hexagonal crystals that interlock with one another and can give rise to materials with high strength and fracture toughness [5, 6].

This study assessed the response of bone to five novel ionomeric glasses, selected with varying calcium to phosphate ratios and heat-treated to crystallize principally apatite, giving essential information to develop this group of materials for biomedical applications.

2. Material and methods

2.1. Glass ceramics

Five glasses were selected for *in vivo* evaluation of bone bonding on the basis of their handling characteristics; that is, they could be cast using the conventional lost wax technique. Three glasses designated LG112, LG113 and LG114 had an ''off apatite'' stoichiometry and form a series based on the formula $4.5SiO_2$–$3Al_2O_3$–YP_2O_5–3CaO–$1.51CaF_2$. The parameter Y was varied to give calcium to phosphate ratios between one and two. LG112 and LG113 being relatively phosphate rich (Ca : P = 1.41 and 1.61, respectively) and LG114 (Ca : P = 1.88) calcium-rich compared to glass LG185 which had the apatite stoichiometry (Ca : P = 1.67). A further phosphate-rich glass LG3 (Ca : P = 1.5) having the composition $4.5SiO_2 3Al_2O_3 1.5P_2O_5 3CaO 1.50CaF_2$ was also included in the study, since this glass has previously given glass–ceramics with high fracture toughness ($> 2.6\,MPa\sqrt{m}$) and high strength (260 MPa) [4] and with its Ca : P ratio being between that of LG112 and LG113, its main compositional difference is a slightly higher fluorite content.

One glass (LG112) was studied in the ''as cast'' or glassy state (designated LG112g). This was also studied following crystallization to principally apatite (LG112a) and to mixed apatite and mullite phases (LG112m). The remaining glasses were evaluated following heat treatment (Table I) and crystallization principally to apatite (LG113a, LG114a, LG185a and LG3a).

Glasses were cast using the lost wax technique to produce solid cylinders nominally 1 mm in diameter. Wax rods were invested in a gypsum investment (Whipmix Cristobalite, Whip-Mix Corporation, Louisville, Kentucky, USA). The molds were heated to 700 °C and held isothermally for 30 min whereupon the temperature was reduced to 590 °C for casting to prevent surface nucleation. The glass was cast at a temperature of 1450 °C, cooled and then crystallized to apatite with a nucleation hold of 1 h and a crystallization hold of 1 h using the temperatures shown in Table I. Additional rods of LG112 were left as glass or crystallized to the mullite phase at a crystallization temperature of 1040 °C. The temperatures selected were based on optimum nucleation temperatures and peak crystallization temperatures determined in previous studies [5, 6].

The rods were de-vested and blasted clean using 50 μm aluminum oxide to remove traces of investment and then cut to short lengths of nominally 2 mm. The short rods were then placed in detergent and cleaned in an ultrasonic bath, then washed twice in butanol and three times in absolute ethanol prior to implantation.

2.2. X-ray diffraction

For X-ray diffraction (XRD), discs of material were produced as described above. Since there was a possibility that the investment material could induce surface nucleation of the glasses giving rise to different proportions of crystal phases at the surface and in the bulk, XRD was carried out on the cast surface and on the bulk material after grinding away approximately 100 μm of the surface. A Philips powder diffractometer (Philips Xpert diffractometer; Philips, Eindhoven, NL) was used with Cu Kα X-rays.

2.3. Implantation

Rods were implanted singly into the mid-shaft of the right femur of weaned (3- to 4-week old) female Wistar rats. Surgery was carried out aseptically under general anesthesia using Halothane in oxygen and nitrous oxide. The shaft of the femur was exposed and under saline irrigation a slow speed round steel dental bur was used to create a hole through the cortex matched to the shape of the implant. A single rod was implanted into each femur to penetrate the marrow cavity and lie flush with the outer cortical surface. Six animals were used for each material and a further six animals were sham operated.

Animals were allowed to recover and were maintained under standard laboratory conditions for 28 days when both left and right femurs were harvested and fixed in 3% gluteraldehyde in 0.1 M cacodylate buffer.

2.4. Electron microscopy/ histomorphometry

Following fixation, specimens were dehydrated through ascending grades of ethanol and embedded in resin (LR White, hard grade; London Resin Co., Reading, UK). Embedded femurs were cut transversely through the implanted rods; the cut surfaces were polished with graded aluminum lapping papers. Blocks were vacuum coated with carbon for backscattered electron mode and viewed with a Philips PSEM 500 scanning electron microscope (SEM).

Energy dispersive analysis of X-rays (EDS) was used to examine the bone surrounding the implants for the presence of ions that may have leached out of the test rods.

Following SEM examination, the blocks were re-polished to remove carbon, then stained en bloc with Stevenols Blue and van Geisons picro fuchsin and examined using conventional light microscopy [7].

SEM photomicrographs of implanted specimens were taken at a magnification of × 30. The pictures were scanned to disc and osseointegration calculated (using Image Pro Plus, Media Cybernetics, USA) as the ratio of the length of the implant within bone to the length of implant in intimate contact with the bone, and expressed as percentage.

SEM examination of unimplanted control rods which had been splutter coated with gold, was undertaken to study the topography of the implant surfaces.

Statistical analysis was undertaken using paired Student's *t*-test.

3. Results

3.1. X-ray diffraction

The heat-treated glasses all crystallized principally to apatite with smaller amounts of secondary crystal phases; these were anorthite, mullite and aluminum phosphate. There was little difference between the bulk XRD and the surface XRD patterns this indicated that the nucleation hold promoted bulk nucleation and that the crystal content of the surface was identical to the bulk. Examination of LG112a showed more apatite to be present in this material in its heat-treated form than for the LG113a and LG114a (Fig. 1). There was possibly a very small amount of apatite in the principally amorphous LG112g (Fig. 2). The main difference between the LG112a and LG112m was as expected with more mullite being present in the samples heated to the mullite crystallization temperature (Fig. 2). The phosphate-rich glass–ceramics (LG112a, LG112m, LG113a and LG3a) all contained small amounts of mullite ($2SiO_2 \cdot 3Al_2O_3$), anorthite ($CaAl_2 \cdot Si_2O_8$) and aluminum phosphate ($AlPO_4$). In contrast, the calcium-rich glass LG114 and the apatite stoichiometry glass contained little or no aluminum phosphate and generally more anorthite. It is assumed that there will be some residual glass left after heat treatment, probably less than 10%. However, this is difficult to quantify from XRD because of masking from the peaks of the crystalline phases.

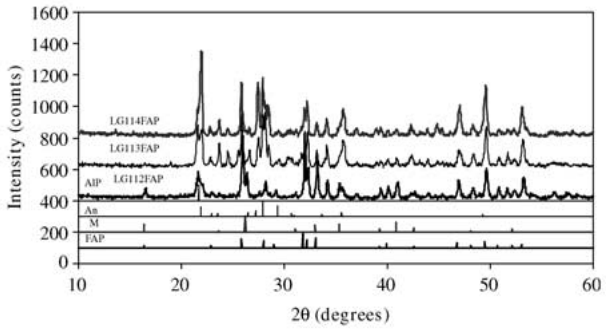

Figure 1 X-ray diffraction patterns for LG114a, LG113a and LG112a. An = anorthite, M = mullite, AIP = aluminum phosphate, FAP = fluorapatite.

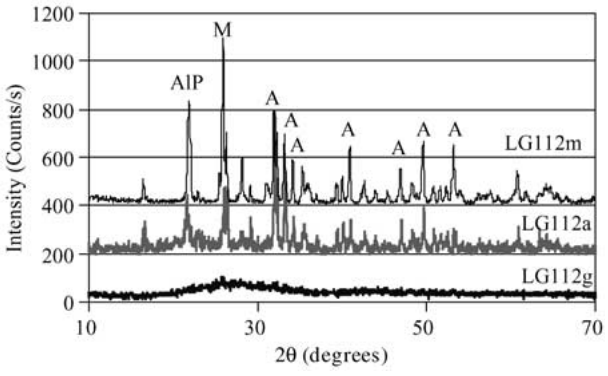

Figure 2 X-ray diffraction patterns of the different phases of LG112. M = mullite, A = apatite, AIP = aluminum phosphate.

3.2. Implantation

Operated limbs appeared sound except for one animal implanted with a rod of LG113a where the femur appeared shortened and deformed and the impression was that the limb had healed following fracture at the surgical site. All remaining femurs appeared clinically similar in size and shape to the unoperated contralateral limb. All sham-operated limbs were clinically sound; visual and radiographic examination failed to reveal evidence of surgical intervention and these limbs were not processed further.

3.3. Electron microscopy/ histomorphometry

SEM examination using backscattered electron imaging revealed new bone had grown around the rods in the cortical region and was in close or intimate contact with the implant. In many cases, the majority of the surface of the implant was covered by new cortical and trabecular bone, which had formed on the surface of the implant and was in intimate contact with it (Figs. 3–5). In places there was intimate contact between the marrow and the implant. Where bone was not in close contact with the implanted material, it did appear to have grown around the implant but was separated from it by an intermediate layer. Ground sections were used in an attempt to determine the nature of the bone–implant interface at a

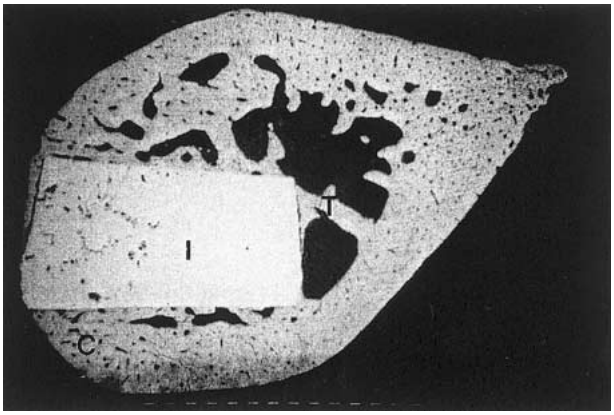

Figure 3 SEM backscatter micrograph of LG114a at 28 days implantation. Original magnification × 30. The scale bars (small white lines) represent 100 μm. This is an example of good osseointegration with new cortical (C) and trabecular (T) bone growth around the implant (I).

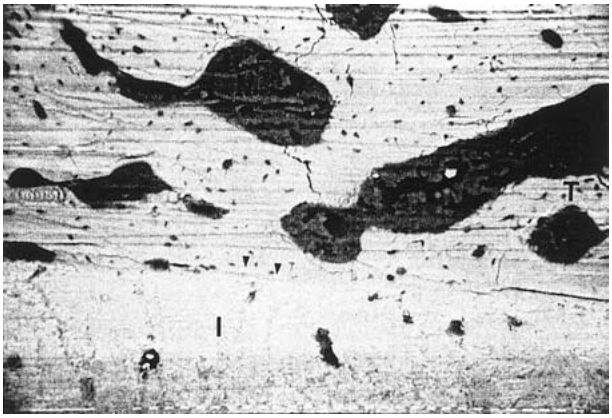

Figure 4 Higher power SEM backscatter micrograph of LG114a at 28 days implantation. Original magnification × 160. The scale bars (small white lines) represent 10 μm. Intimate contact (arrow heads) between implant (I) and trabecular bone (T) is evident; marrow spaces (M) can be seen.

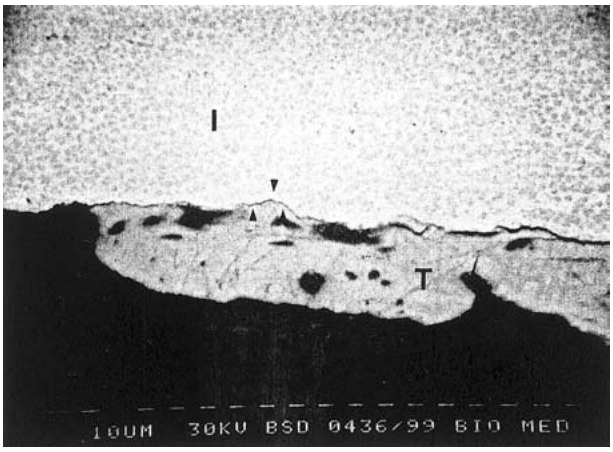

Figure 5 SEM micrograph showing LG112a at 28 days implantation. Original magnification × 320. The scale bars (small white lines) represent 10 μm. There is intimate contact (arrow heads) between implant (I) and trabecular bone (T). Marrow (M) is present.

cellular level. Where the SEM images showed intimate contact between bone and implant, this was confirmed by light microscopy. Where there was an apparent failure of integration in LG113a and LG112g (Fig. 6), cellular material was interposed between implant and bone; this

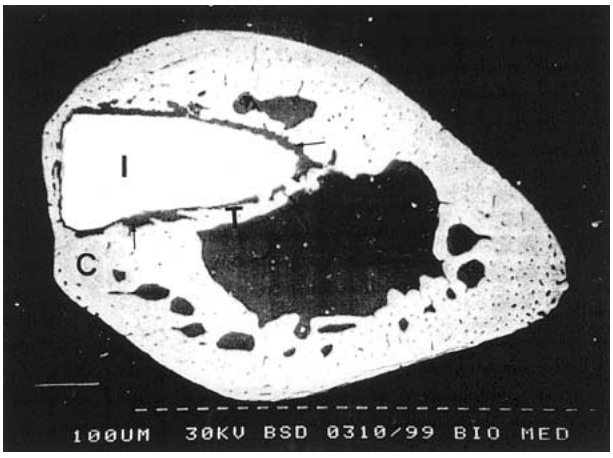

Figure 6 SEM micrograph showing LG113a at 28 days implantation. This is an example of poor integration, a significant gap (arrows) can be seen between the implant (I) and both cortical and trabecular bone (C and T). Original magnification × 30, the scale bars (small white lines) represent 100 μm.

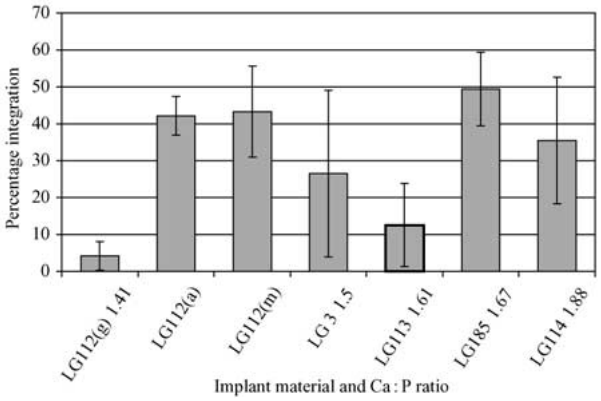

Figure 7 Bar chart showing percentage osseointegration of LG112, LG113, LG114, LG185 and LG3 in the apatite forms of the materials (a) and LG112 in its glass (g) and mixed apatite–mullite (m) forms.

took the form of chronic inflammatory cells resembling macrophages and multinucleate cells, osteoid and some fibrous connective tissue. In situations where there was a very slight gap between the rod and bone, as seen in the SEM images, this appeared to be processing artefact since there was no evidence of interposed soft tissues using optical microscopy.

Overall, the materials could be divided into two groups according to whether or not there was integration with bone. The good integrators comprised LG112a, LG112m, LG114a and LG185a and there was no statistically significant difference between the members of this group. The poor integrators comprised LG112g and LG113a, between which there was no statistically significant difference. However, there were significant differences between all the good integrators and both poor integrators ($p < 0.01$ to $p < 0.0001$). LG3 did not differ significantly from either the good or poor integrators (Fig. 7).

SEM examination of the control rods revealed a mixed and varied surface topography with the good integrators exhibiting a generally rough and almost porous surface appearance (Fig. 8(a)). The poor integrator, LG112g, appeared smooth and non-porous, and LG113a, the second poor integrator, had a partly crystalline surface interspersed among areas of an amorphous nature (Fig. 8(b)). The surface features of LG3 were intermediate between those of the good and poor integrators.

EDS of bone surrounding the implants failed to reveal the presence of silicon or aluminum ions. Calcium and phosphorus was identified in bone surrounding the implanted rods. However, no quantitative assessment of calcium and phosphate content was made and therefore any subtle differences in mineralization density were not detected.

4. Discussion

The rat femur healing bone model provides information on the response of growing bone to biomaterials. Although it may not accurately reflect the likely clinical situation in adult humans, it is a relatively simple means of assessing response prior to further assessment in more rigorous models, such as the non-healing rat ramus model or in larger animals [8].

All materials, with the exception of LG112g and

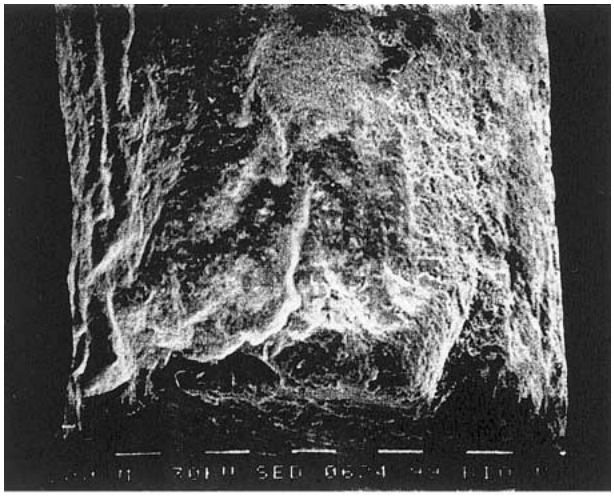

(a)

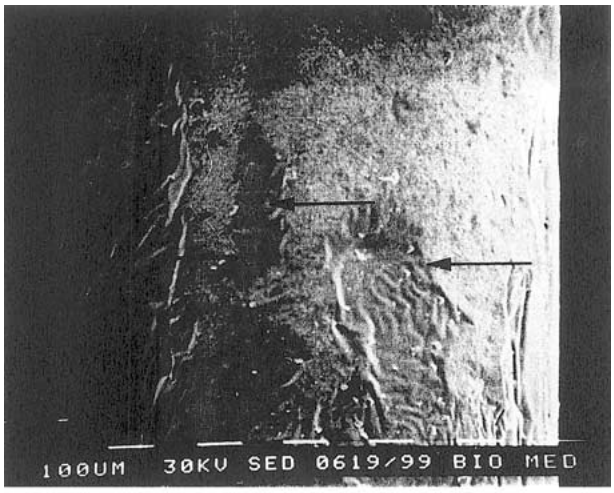

(b)

Figure 8 SEM micrographs to show surface topography of unimplanted rods. LG185a, a good integrator, has a consistently rough surface (a), whereas LG113a, a poor integrator (b), has a more varied surface with apparently smooth areas (arrows). Original magnification × 80.

LG113a, elicited a favorable response from the healing bone with encapsulation of the implant by bone (Figs. 3–5). There was clear evidence of intimate bone to implant contact at both SEM (Figs. 4 and 5) and light microscope levels with minimal fibrous tissue encapsulation or chronic inflammation. These materials appear to be well tolerated in bone, at least in the short term. Poor integration and the presence of chronic inflammation were associated with the amorphous sample (LG112g). This was significantly different to the response induced by LG112a, crystallization to principally apatite or to a mixed apatite and mullite phase (LG112m). Thus, it appears that crystallization improved the biocompatibility of this material

X-ray diffraction was available for LG112g, LG112a, LG112m, LG113a and LG114a and it was clear that LG112g was almost completely amorphous and there was less apatite in LG113a and LG114a than in LG112a (Figs. 1 and 2). The different biological responses seen between LG112a and LG114a was not significant and was due to the large standard deviations in our sample (Fig. 7). A chronic inflammatory reaction was also associated with LG112g implants. This could be a reaction to the lack of integration or a cause of the lack of integration. Reduction in solubility following crystallization of the glass could be a causative factor in the differences seen, as could the difference in apatite/mullite content of the implants.

Gross examination of the surface of control implants using the SEM revealed some differences, notably that the poor integrators appeared smoother than the good integrators (Fig. 8(a) and (b)). The different surface topography may reflect differences in crystallization, which could influence cell attachment and the biological response induced [9]. A noticeable feature of LG113a was the presence of areas resembling the smoother glassy surface of LG112g. It is possible that there was a higher proportion of residual glass in the LG113a implants. The residual glass phase in the surface of LG113a could also have been less stable resulting in a more degradable implant. The glass phase would also be more capable of releasing aluminum ions which are known to promote osteoid formation and inhibit bone mineralization [10]. Particulate material shed from implants may also account for a chronic inflammatory response as seen around the rods of LG112g and LG113a. However, no aluminum was detected in the immediate vicinity of the implants using EDAX, though soluble ions may have been lost during processing and the sensitivity of EDAX to aluminum may have been inadequate if only very small quantities were present.

The lower apatite content of LG113a may also account for its poor osseointegration. In these respects, the LG113a sample is closer to the LG112g in that both of these materials elicited a similar biological response (Fig. 7). There is much less fluorapatite in LG113a and LG114a than in LG112a, which would suggest that the degradability of the residual glass phase and solubility of secondary crystalline phases are possibly the dominant factors in determining the osseointegration of the LG113a sample. In contrast, the response of the apatite stoichiometric implant, LG185a which could be expected to be more stable on implantation, [11] was found to be favorable (Fig. 5). Further work using slam frozen specimens and solubility studies may shed more light on the mechanisms influencing the biological response induced.

5. Conclusions

- Crystallizing LG112 to apatite or apatite–mullite significantly improved bone response.
- A crystalline surface containing a large proportion of fluorapatite is more likely to favor bone bonding.
- Surface roughness, residual glass content and solubility may be significant factors affecting integration.
- None of the materials tested adversely affected bone mineralization.
- LG112 and LG185 appear worthy of more detailed investigation as potential bone substitutes.

Acknowledgments

We wish to thank Mr John Procter of the Department of Biomedical Sciences at the University Of Sheffield for

technical assistance with scanning electron microscopy. The authors would like to thank the European Commission for funding under the Brite EuRam Scheme Contract Number Contract BRPR-CT96-0230.

References

1. A. RAFFERTY, A. CLIFFORD, R. HILL, D. WOOD, B. SAMUNEVA and M. DIMITROVA-LUKACS, *J. Am. Ceram. Soc.* **83** (2000) 2833.
2. K. K. JOHAL, G. MENDOZA-SUAREZ, J. I. ESCALANTE-GARCIA, R. G. HILL and I. M. BROOK, *J. Mater. Sci. Mater. Med.* **13** (2002) 375.
3. R. T. RAMSDEN, R. C. D. HEARDMAN and R. H. LYLE, *J. Laryng. Otol.* **106** (1992) 949.
4. A. JOHNSON, M. Y. SHAREEF, J. M. WALSH, P. V. HATTON, R. VAN NOORT and R. G. HILL, *Dent. Mater.* **14** (1998) 412.
5. A. CLIFFORD, R. G. HILL, A. RAFFERTY, P. MOONEY, D. WOOD, B. SAMUNEVA and S. MATUSUYA, *J. Mater. Sci.: Mater. Med.* **12** (2001) 461.
6. A. CLIFFORD, R. G. HILL, M. J. TOWLER and D. J. WOOD, *J. Mater. Sci.* **36** (2001) 3955.
7. C. MANIATOPOULOS, A. RODRIGUEZ, D. A. DEPORTER, D. PERIO and A. H. MELCHER, *Int. J. Oral Maxillofac. Implants* **1** (1986) 31.
8. L. A. SALATA, G. T. CRAIG and I. M. BROOK, *ibid.* **13** (1998) 44.
9. P. DUCHEYNE and Q. QUI, *Biomaterials* **20** (1999) 2287.
10. H. CARTER, P. SLOAN, I. M. BROOK and P. V. HATTON, *ibid.* **18** (1997) 459.
11. J. C. KNOWLES and W. BONFIELD, *J Biomed. Mater. Res.* **12** (1993) 1591.

Received 12 August 2002
and accepted 17 April 2003